Supporting Information for

Rational Microstructure Design of SnS_2-Carbon Composites for Superior Sodium Storage Performance

Yi Zhao,[a] Binbin Guo,[a] Qianqian Yao,[a,b] Jiaxin Li,[a] Jianshuo Zhang,[a,b] Kun Hou,[a] and Lunhui Guan*[a]

[a]CAS Key Laboratory of Design and Assembly of Functional Nanostructures, Fujian Key Laboratory of Nanomaterials, Fujian Institute of Research on the Structure of Matter, Chinese Academy of Sciences, Fuzhou 350108, China.
E-mail: guanlh@fjirsm.ac.cn

[b]University of Chinese Academy of Sciences, Beijing, 100049, China

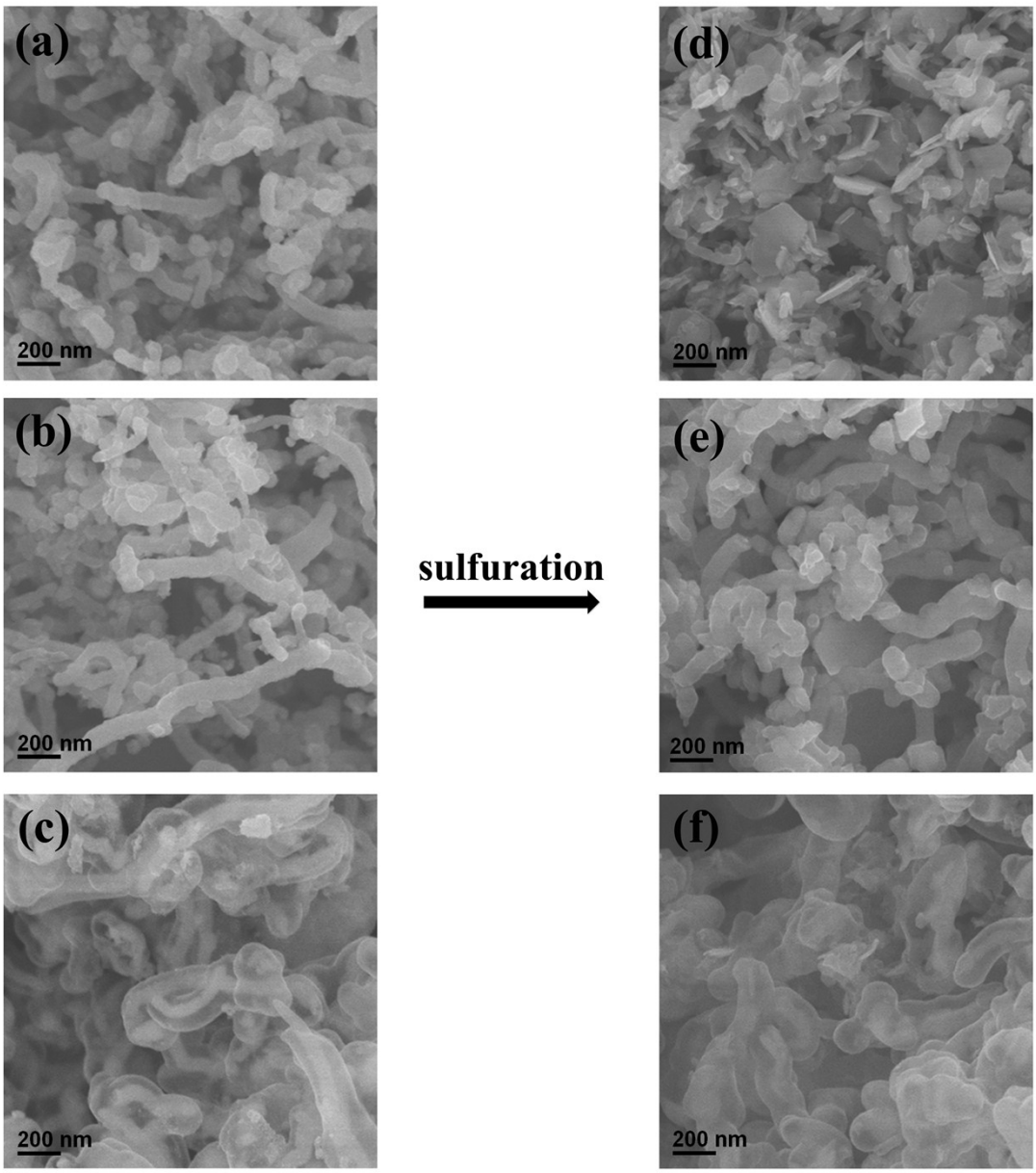

Fig. S1 SEM images of (a) MWNT@SnO_2, (b) MWNT@SnO_2@C, (c) MWNT@SnO_2@void@C, (d) MWNT@SnS_2 NS, (e) MWNT@SnS_2@C, and (f) MWNT@SnS_2 NS@C composites.

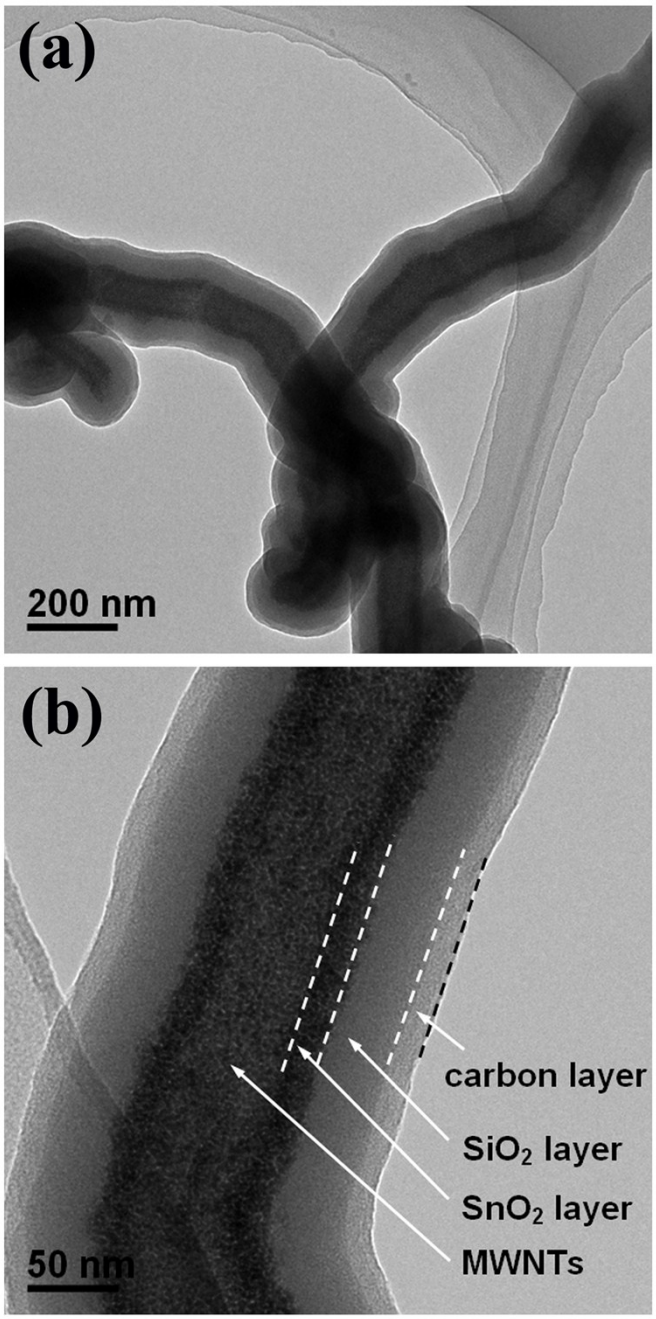

Fig. S2 TEM images of MWNT@SnO_2@SiO_2@C composites. As can be seen, MWNTs were sequentially coated with SnO_2, SiO_2, and carbon layers.

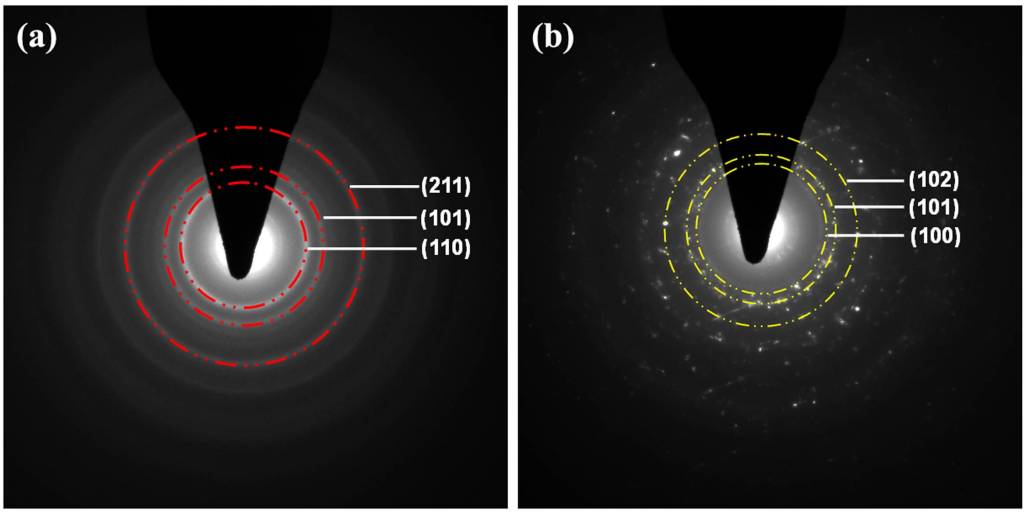

Fig. S3 Selected area electron diffraction (SAED) patterns of (a) MWNT@SnO_2@void@C, and (b) MWNT@SnS_2 NS@C composites, from which the diffraction rings can be well assigned to tetragonal SnO_2 and hexagonal SnS_2, respectively.

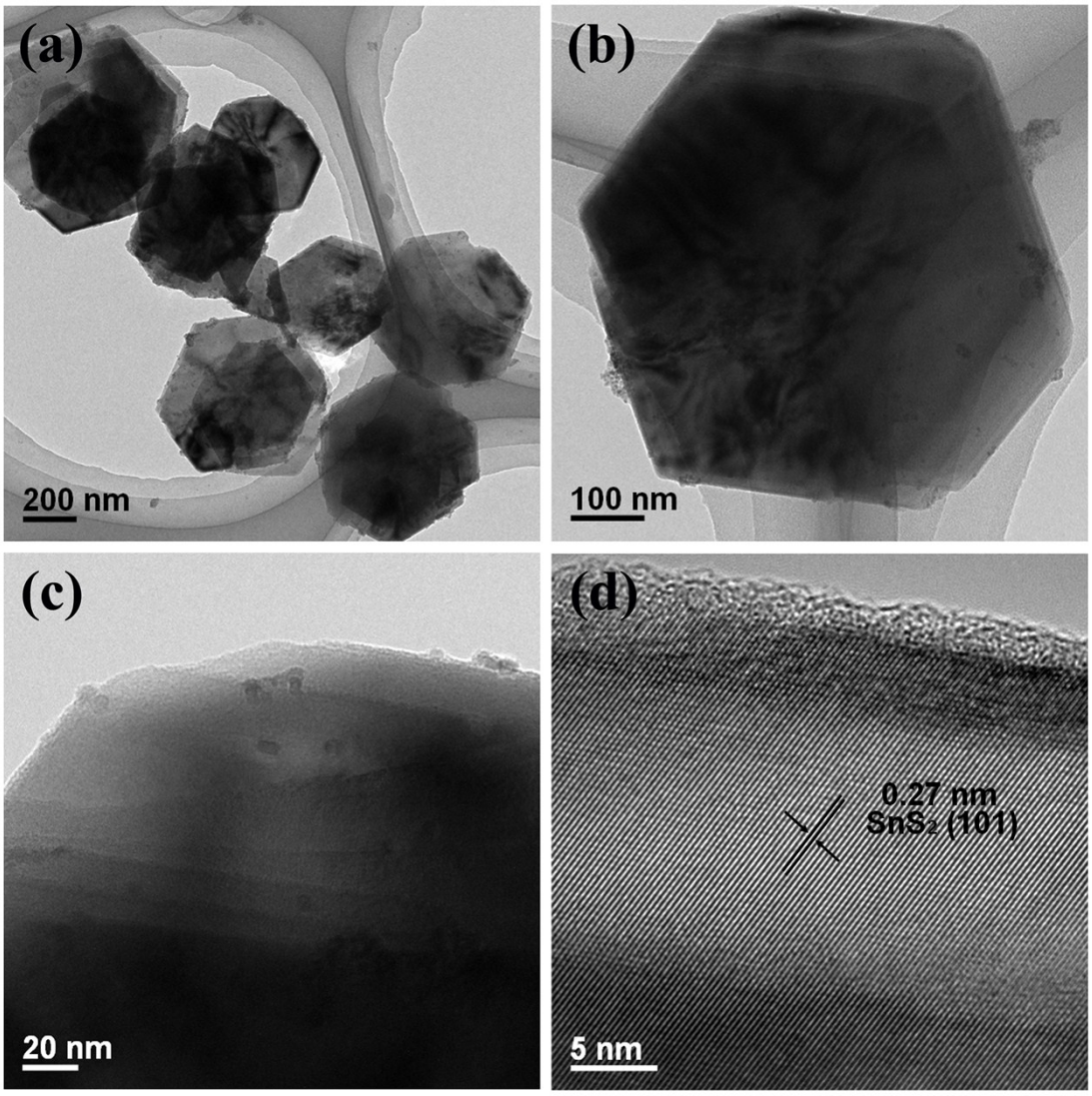

Fig. S4 TEM images of pure SnS_2 nanosheets. The hydrothermal synthesized SnS_2 NS exhibited large lateral size of 400-600 nm and thickness around 90 nm. The interplanar spacing of 0.27 nm in Fig. S3d could be assigned to the (101) plane of hexagonal SnS_2.

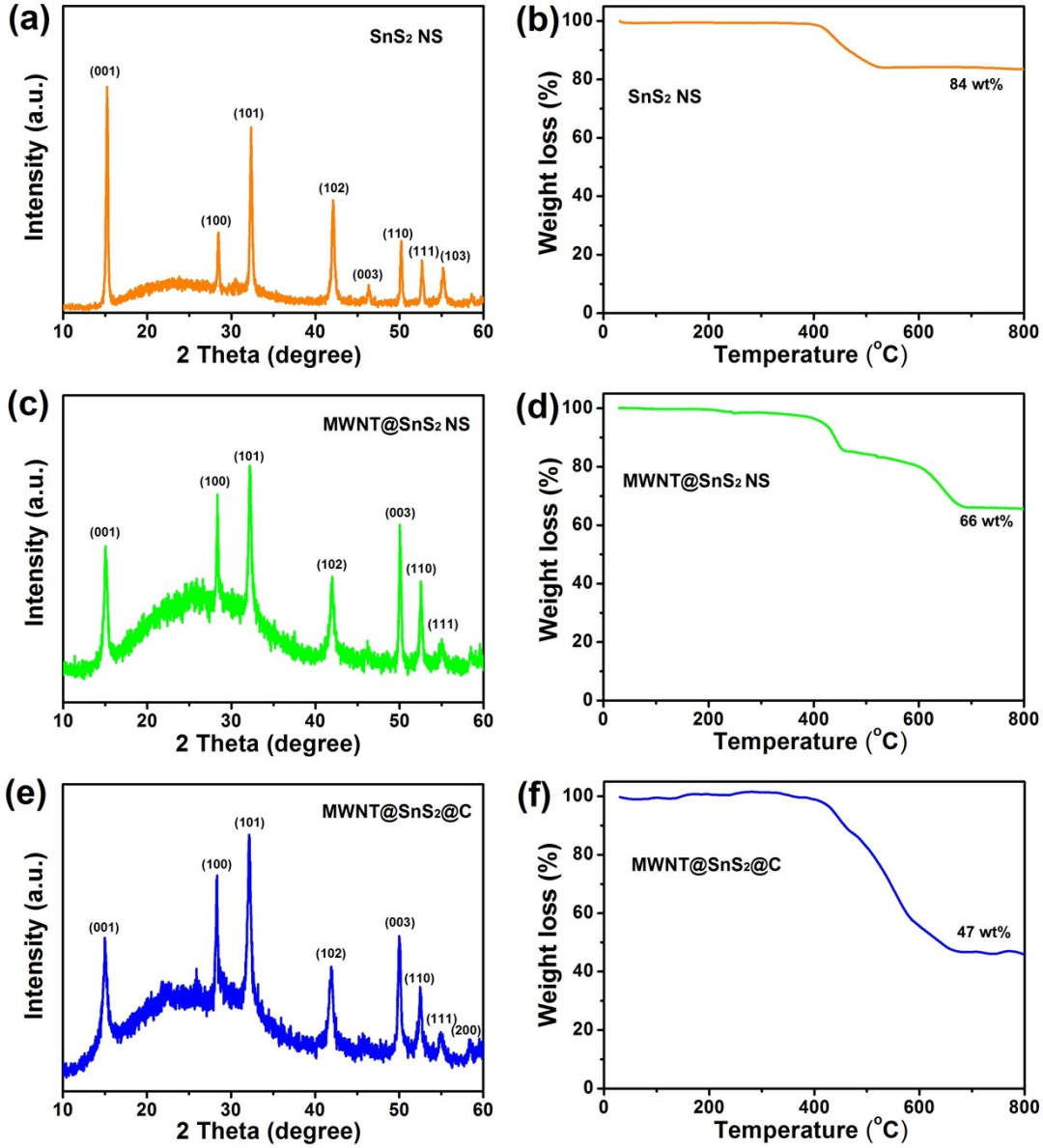

Fig. S5 (a, c, e) XRD patterns, and (b, d, f) TGA curves of (a-b) pure SnS_2 NS, (c-d) MWNT@SnS_2 NS, and (e-f) MWNT@SnS_2@C composite. The XRD patterns of these three sample were well indexed to the hexagonal SnS_2 (JCPDS No.23–0677). Seen from the TGA curve of pure SnS_2 NS in Fig. S3b, one weight loss region from 400-530 ^oC was resulted from the oxidation of SnS_2 to SnO_2. The weight content of SnS_2 was almost 100%. In Fig. S3d, two regions at 400-500 ^oC and 500-690 ^oC were ascribed to the oxidation of SnS_2 and weight loss of MWNTs, respectively. The weight content of SnS_2 in MWNT@SnS_2 composite was around 80 wt%. For MWNT@SnS2@C, there were three temperature regions at 390-470 ^oC, 470-570 ^oC, and 570 to 680 ^oC, corresponding to the formation of SnO_2, removal of carbon layer, and MWNTs, respectively. The final content of SnS_2 in MWNT@SnS_2@C composite was around 57 wt%.

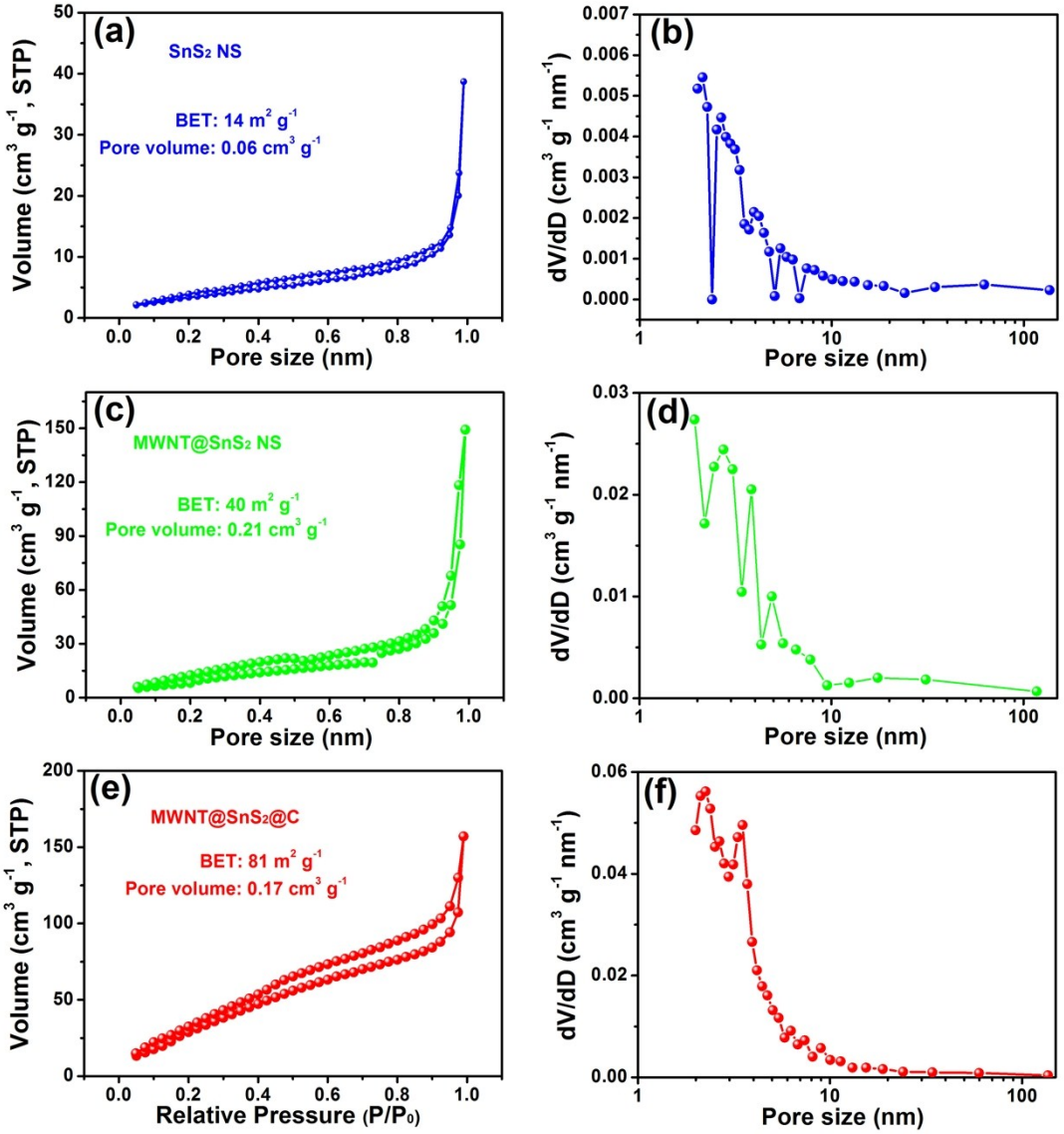

Fig. S6 (a, c, e) Nitrogen adsorption—desorption isotherms, and (b, d, f) pore size distribution curves of (a-b) SnS_2 NS, (c-d) MWNT@SnS_2 NS, and (e-f) MWNT@SnS_2@C composites.

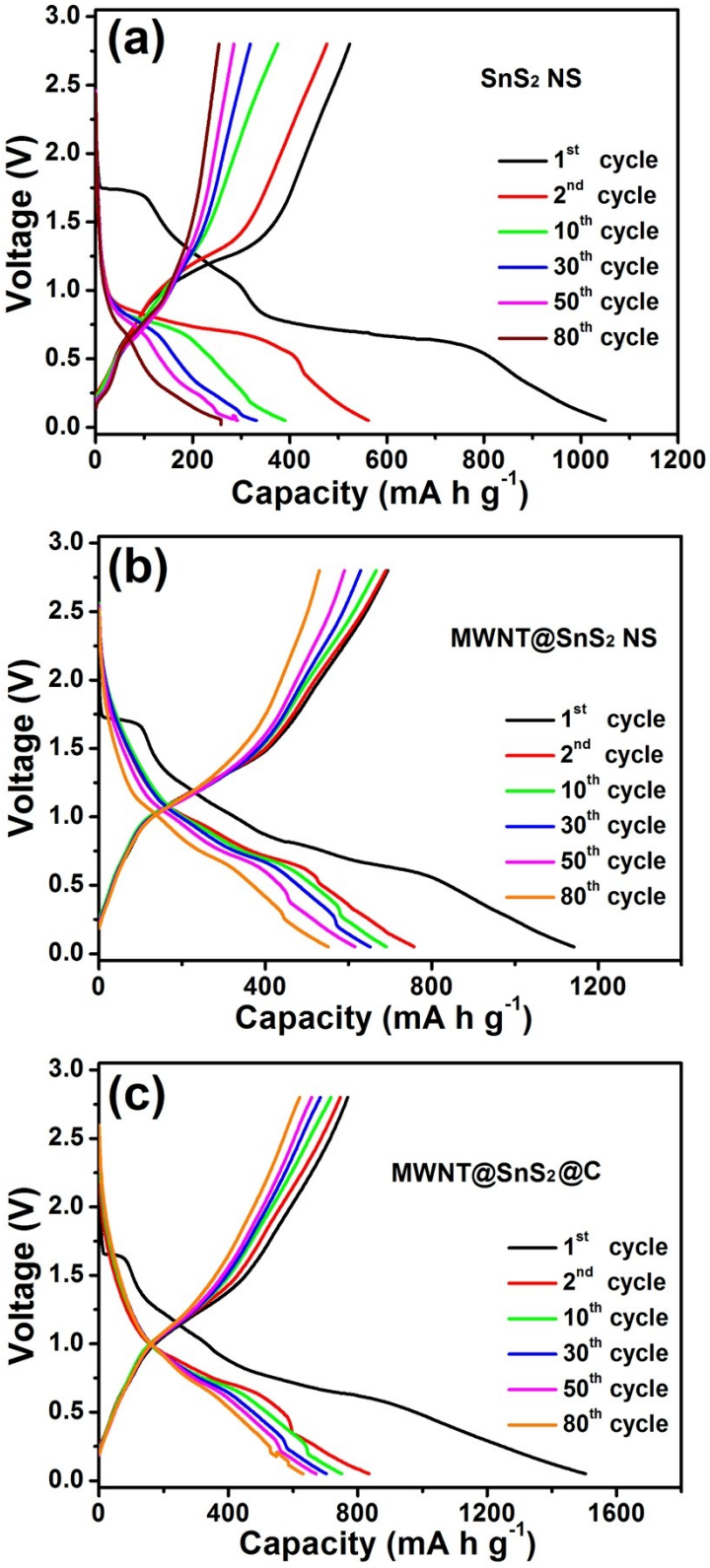

Fig. S7 Selected discharge-charge profiles of (a) SnS_2 NS, (b) MWNT@SnS_2 NS, and (c) MWNT@SnS_2@C electrodes at a current density of 100 mA g^{-1}.

Table S1. Electrochemical performance of carbon-SnS_2 composites as anode materials for NIBs.

Materials	Current density (mA g^{-1})	Cycle Number	Capacity (mAh g^{-1})	Reference
Graphene-SnS_2 nanosheets	0.2	100	630	[1]
Graphene-SnS_2 nanoplates	0.02	60	670	[2]
Graphene-SnS_2 nanoparticles	0.05	50	610	[3]
SnS_2 nanosheets	0.1	50	647	[4]
Graphene-SnS_2	0.2	300	509	[5]
Graphene-SnS_2 nanoplates	0.2	100	619	[6]
Graphene-SnS_2 nanocrystals	0.2	100	680	[7]
N-doped graphene-SnS_2 nanoparticles	0.2	100	450	[8]
Graphene-SnS_2	0.1	100	826	[9]
Graphene-SnS_2 nanocrystals	1	100	418	[10]
Carbon nanotube-SnS_2 nanosheets	0.1	100	660	[11]
Carbon nanotube-SnO_2-SnS_2	0.05	100	355	[12]
MWNT@SnS_2 NS@C	**0.1**	**100**	**710**	**Our work**

1. B. H. Qu, C. Z. Ma, G. Ji, C. H. Xu, J. Xu, Y. S. Meng, T. H. Wang and J. Y. Lee, *Adv Mater*, 2014, **26**, 3854-3859.
2. X. Q. Xie, D. W. Su, S. Q. Chen, J. Q. Zhang, S. X. Dou and G. X. Wang, *Chem-Asian J*, 2014, **9**, 1611-1617.
3. P. V. Prikhodchenko, D. Y. W. Yu, S. K. Batabyal, V. Uvarov, J. Gun, S. Sladkevich, A. A. Mikhaylov, A. G. Medvedev and O. Lev, *J Mater Chem A*, 2014, **2**, 8431-8437.
4. W. P. Sun, X. H. Rui, D. Yang, Z. Q. Sun, B. Li, W. Y. Zhang, Y. Zong, S. Madhavi, S. X. Dou and Q. Y. Yan, *Acs Nano*, 2015, **9**, 11371-11381.
5. Y. D. Zhang, P. Y. Zhu, L. L. Huang, J. Xie, S. C. Zhang, G. S. Cao and X. B. Zhao, *Adv Funct Mater*, 2015, **25**, 481-489.

6. Y. C. Liu, H. Y. Kang, L. F. Jiao, C. C. Chen, K. Z. Cao, Y. J. Wang and H. T. Yuan, *Nanoscale*, 2015, **7**, 1325-1332.
7. Y. Jiang, M. Wei, J. K. Feng, Y. C. Ma and S. L. Xiong, *Energ Environ Sci*, 2016, **9**, 1430-1438.
8. Y. Jiang, Y. Z. Feng, B. J. Xi, S. S. Kai, K. Mi, J. K. Feng, J. H. Zhang and S. L. Xiong, *J Mater Chem A*, 2016, **4**, 10719-10726.
9. F. Z. Tu, X. Xu, P. Z. Wang, L. Si, X. S. Zhou and J. C. Bao, *J Phys Chem C*, 2017, **121**, 3261-3269.
10. Y. Liu, Y. Z. Yang, X. Z. Wang, Y. F. Dong, Y. C. Tang, Z. F. Yu, Z. B. Zhao and J. S. Qiu, *Acs Appl Mater Inter*, 2017, **9**, 15484-15491.
11. H. M. Li, M. Zhou, W. Li, K. L. Wang, S. J. Cheng and K. Jiang, *Rsc Adv*, 2016, **6**, 35197-35202.
12. S. G. Zhang, H. Q. Zhao, L. C. Yue, Z. Y. Wang and J. Mi, *J Alloy Compd*, 2017, **717**, 127-135.

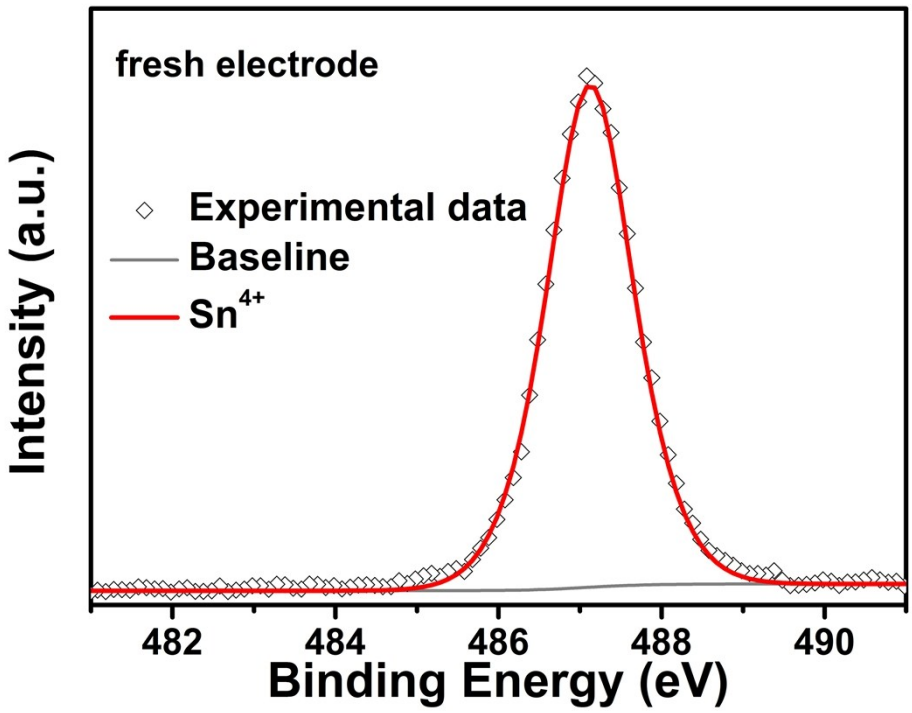

Fig. S8 High-resolution Sn $3d_{5/2}$ XPS spectra of fresh MWNT@SnS_2 NS electrode. The binding energies of Sn $3d_{5/2}$ before cycle was located at 487.1 eV, in consistent with the data for Sn $3d_{5/2}$ in SnS_2.

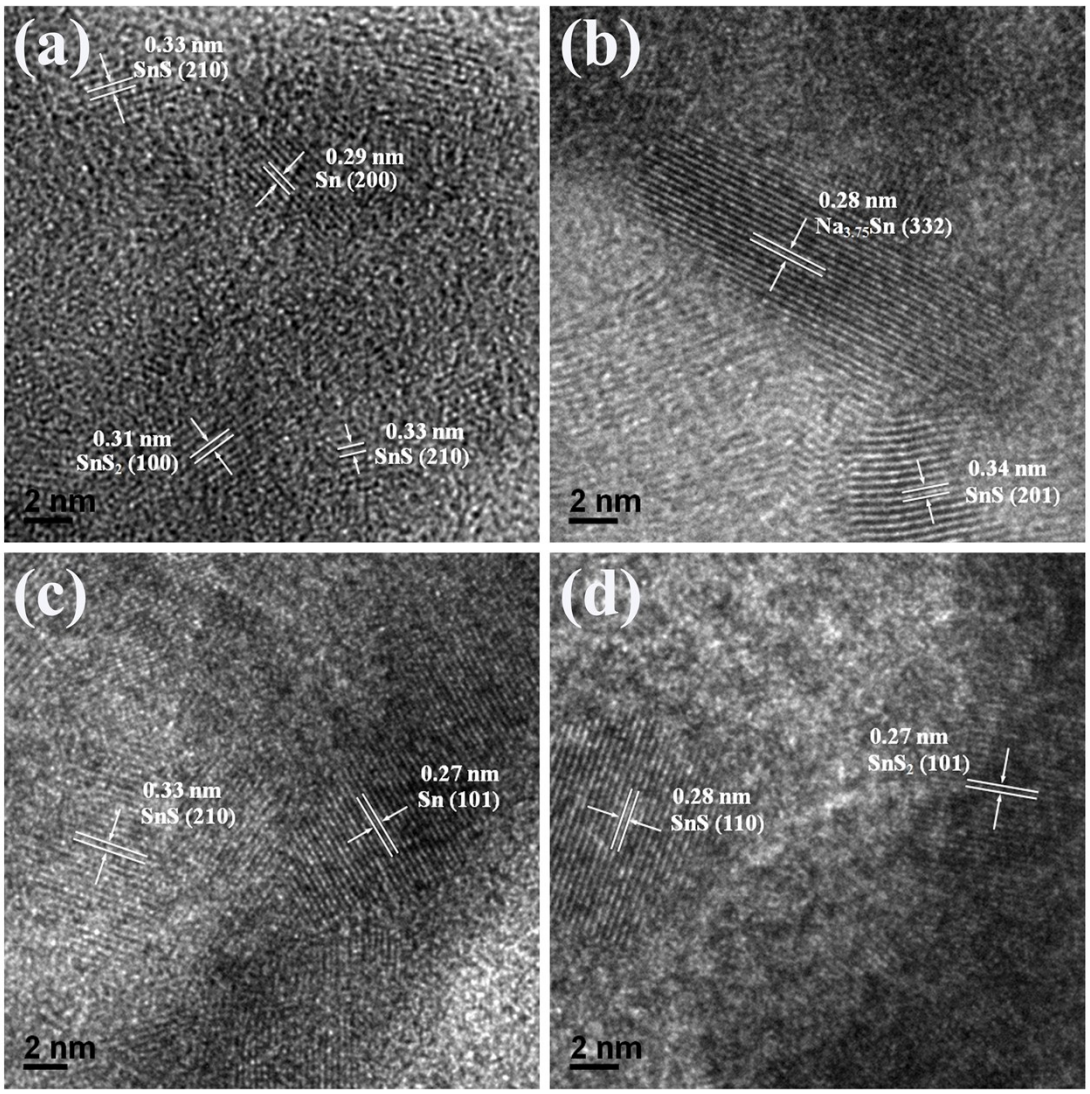

Fig. S9 HRTEM images of MWNT@SnS_2 NS@C electrode after first discharge to 0.6 V (a), after first discharge to 0.05 V (b), after first charge to 1.5 V (c), and first charge to 2.8 V (d).

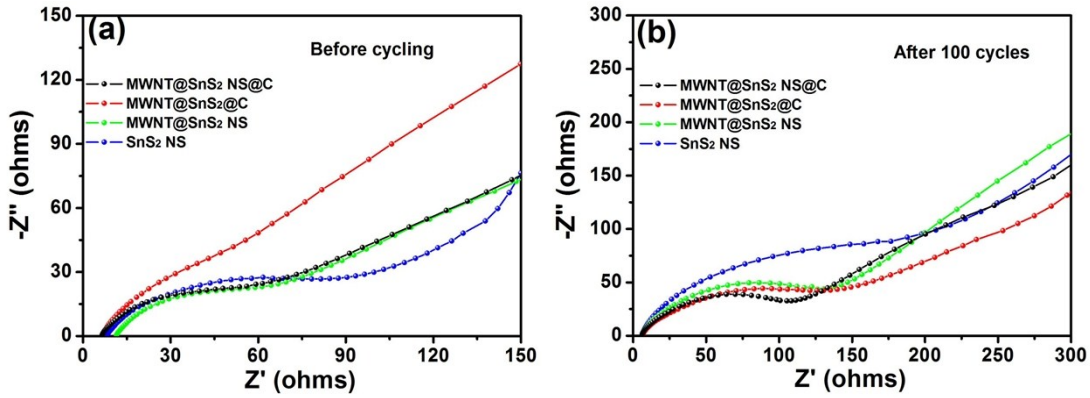

Fig. S10 EIS profiles of SnS_2 NS, MWNT@SnS_2 NS, MWNT@SnS_2@C, and MWNT@SnS_2 NS@C electrodes before cycling (a) and after 100 cycles (b).